Extended Fano model of Extraordinary Electromagnetic Transmission through subwavelength hole arrays in the terahertz domain

Jean-Baptiste Masson[1], **Alexander Podzorov, Guilhem Gallot**

Laboratoire d'Optique et Biosciences, École Polytechnique, CNRS, 91128 Palaiseau, France
INSERM U696, 91128 Palaiseau, France
Guilhem.Gallot@polytechnique.edu

Abstract: We developed an extended Fano model describing the Extraordinary Electromagnetic Transmission (EET) through arrays of subwavelength apertures, based on terahertz transmission measurements of arrays of various hole size and shapes. Considering a frequency-dependent coupling between resonant and non-resonant pathways, this model gives access to a simple analytical description of EET, provides good agreement with experimental data, and offers new parameters describing the influence of the hole size and shape on the transmitted signal.

OCIS codes: (050.6624) Subwavelength structures; (050.1940) Diffraction and gratings : Diffraction; (260.3090) Infrared, far.

References and links

1. T. W. Ebbesen, H. J. Lezec, H. F. Ghaemi, T. Thio, and P. A. Wolff, "Extraordinary optical transmission through sub-wavelength hole arrays," Nature **391**, 667–668 (1998).
2. W. L. Barnes, A. Dereux, and T. W. Ebbesen, "Surface plasmon subwavelength optics," Nature **424**, 824–830 (2003).
3. E. Ozbay, "Plasmonic: merging photonics and electronics at nanoscale dimensions," Science **311**, 189–193 (2006).
4. H. Liu and P. Lalanne, "Microscopic theory of the extraordinary optical transmission," Nature **452**, 728–731 (2008).
5. J. B. Pendry, L. Martin-Moreno, and F. J. Garcia-Vidal, "Mimicking Surface Plasmons with Structured Surfaces," Science **305**, 847–848 (2004).
6. C. Genet and T. W. Ebbesen, "Light in tiny holes," Nature **445**, 39–46 (2007).
7. L. Martin-Moreno, F. J. Garcia-Vidal, H. J. Lezec, K. M. Pellerin, T. Thio, J. B. Pendry, and T. W. Ebbesen, "Theory of Extraordinary Optical Transmission through Subwavelength Hole Arrays," Phys. Rev. Lett. **86**(6), 1114–1117 (2001).
8. P. Lalanne, J. P. Hugonin, and J. C. Rodier, "Theory of Surface Plasmon Generation at Nanoslit Apertures," Phys. Rev. Lett. **95**, 263,902 (2005).
9. J. Bravo-Abad, A. I. Fernandez-Dominguez, F. J. Garcia-Vidal, and L. Martin-Moreno, "Theory of Extraordinary Transmission of Light through Quasiperiodic Arrays of Subwavelength Holes," Phys. Rev. Lett. **99**, 203,905 (2007).
10. G. Gay, O. Alloschery, B. V. de Lesegno, C. O'Dwyer, J. Weiner, and H. J. Lezec, "The optical response of nanostructured surfaces and the composite diffracted evanescent wave model," Nature Physics **2**, 262–267 (2006).
11. K. G. Lee and Q. H. Park, "Coupling of Surface Plasmon Polaritons and Light in Metallic Nanoslits," Phys. Rev. Lett. **95**, 103,902 (2005).

[1]Now with Institut Pasteur, CNRS URA 2171, Unit In Silico Genetics, 75724 Paris Cedex 15, France

#111238 - $15.00 USD Received 11 May 2009; revised 30 Jun 2009; accepted 30 Jun 2009; published 14 Aug 2009

12. D. Qu and D. Grischkowsky, "Observation of a New Type of THz Resonance of Surface Plasmons Propagating on Metal-Film Hole Arrays," Phys. Rev. Lett. **93**(19), 196,804 (2004).
13. J. M. Brok and H. P. Urbach, "Extraordinary transmission through 1, 2 and 3 holes in a perfect conductor, modelled by a mode expansion technique," Opt. Exp. **14**(7), 2552–2572 (2006).
14. A. Agrawal, Z. V. Vardeny, and A. Nahata, "Engineering the dielectric function of plasmonic lattices," Opt. Exp. **16**(13), 9601–9613 (2008).
15. A. P. Hibbins, J. R. Sambles, C. R. Lawrence, and J. R. Brown, "Squeezing MillimeterWaves into Microns," Phys. Rev. Lett. **92**(14), 143,904 (2004).
16. C. Genet, M. P. van Exter, and J. P. Woerdman, "Fano-type interpretation of red shifts and red tails in hole array transmission spectra," Opt. Comm. **225**(4-6), 331–336 (2003).
17. M. Sarrazin, J.-P. Vigneron, and J.-M. Vigoureux, "Role of Wood anomalies in optical properties of thin metallic films with a bidimensional array of subwavelength holes," Phys. Rev. B **67**, 085,415 (2003).
18. S.-H. Chang, S. K. Gray, and G. C. Schatz, "Surface plasmon generation and light transmission by isolated nanoholes and arrays of nanoholes in thin metal films," Opt. Exp. **13**(8), 3150–3165 (2005).
19. W. Zhang, A. K. Azad, J. Han, J. Xu, J. Chen, and X.-C. Zhang, "Direct Observation of a Transition of a Surface Plasmon Resonance from a Photonic Crystal Effect," Phys. Rev. Lett. **98**, 183,901 (2007).
20. J.-B. Masson and G. Gallot, "Coupling between surface plasmons in subwavelength hole arrays," Phys. Rev. B **73**, 121,401(R) (2006).
21. U. Fano, "Effects of configuration interaction on intensities and phase shifts," Phys. Rev. **124**(6), 1866–1875 (1961).
22. J. Han, A. K. Azad, M. Gong, X. Lu, and W. Zhang, "Coupling between surface plasmons and nonresonant transmission in subwavelength holes at terahertz frequencies," Appl. Phys. Lett. **91**, 071,122 (2007).
23. S. Bandopadhyay, B. Dutta-Roy, and H.S.Mani, "Understanding the Fano Resonance : through Toy Models," Am. J. Phys. **72**, 1501 (2004).
24. C.-M. Ryu and S. Y. Cho, "Phase evolution of the transmission coefficient in an Aharonov-Bohm ring with Fano resonance," Phys. Rev. B **58**(7), 3572 (1998).
25. H. A. Bethe, "Theory of diffraction by small holes," Phys. Rev. **66**(7-8), 163–182 (1944).
26. C. J. Bouwkamp, "Diffraction theory," Rep. Prog. Phys. **17**, 35–100 (1954).
27. D. Grischkowsky, S. R. Keiding, M. van Exter, and C. Fattinger, "Far-infrared time-domain spectroscopy with terahertz beams of dielectrics and semiconductors," J. Opt. Soc. Am. B **7**(10), 2006–2015 (1990).
28. C.-C. Chen, "Transmission of microwave through perforated flat plates of finite thickness," IEEE Trans. Microwave Theo. Tech. **21**(1), 1–6 (1973).
29. J.-B. Masson, A. Podzorov, and G. Gallot, "Anomalies in the disappearance of the extraordinary electromagnetic transmission in subwavelength hole arrays," Opt. Exp. **16**(7), 4719–4730 (2008).
30. B. D. Fried and S. D. Conte, *The plasma dispersion function. The Hilbert transform of the Gaussian* (Academic Press, New York, 1961).
31. C. Cohen-Tannoudji, B. Diu, and F. Laloe, *Quantum Mechanics* (Wiley and Hermann, Paris, 1977).
32. D. G. Duffy, "On the numerical inversion of Laplace transforms: comparison of three new methods on characteristic problems from applications," ACM Trans. Math Soft. **19**(3), 333–359 (1993).
33. K. F. Riley, M. P. Hobson, and S. J. Bence, *Mathematical methods for physics and engineering* (Cambridge University Press, 2006).
34. W. H. Press, S. A. Teukolsky, W. T. Vetterling, and B. P. Flannery, *Numerical recipes in C* (Cambridge University Press, Cambridge, 1992).

1. introduction

Interaction between metal surface waves and periodic geometry of subwavelength structures is at the core of the recent but crucial renewal of interest in plasmonics [1, 2, 3, 4] from which major promising applications in optics and electronics are arising, based in particular on the Extraordinary Electromagnetic Transmission (EET) through periodic subwavelength structures. This renewal has raised considerable interest and subsequent theoretical discussions as to describe this abnormal transmission, leading to numerous concurrent theories.

EET is characterized by abnormally high asymmetrical resonances of light transmission through arrays of subwavelength apertures for wavelengths close to the period of the arrays. EET has been observed over the full electromagnetic range, from visible to terahertz and microwave, therefore even for almost perfectly conductive metals [3, 5]. The microscopic nature of EET is still debated but Surface Plasmon Polaritons (SPP) seem to play a major role in the visible and near infrared range. When dealing with highly conductive metals such as in the far

#111238 - $15.00 USD Received 11 May 2009; revised 30 Jun 2009; accepted 30 Jun 2009; published 14 Aug 2009

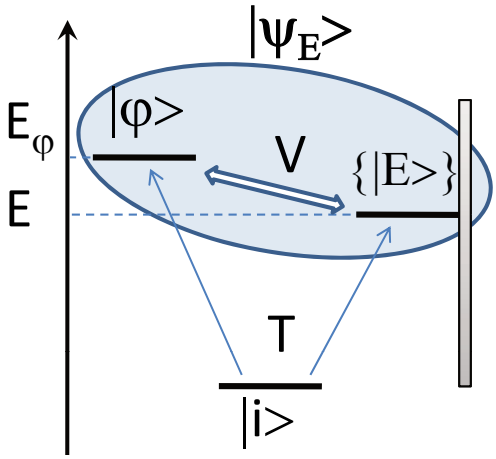

Fig. 1. Fano model of a subwavelength hole array and the coupling V between a continuum of states $\{|E\rangle\}$ and a resonant level E_φ. $|i\rangle$ and $|\psi_E\rangle$ are the initial and final states, respectively.

infrared, importance of SPP is suspected to disappear, and may be replaced by surface waves such as quasi-cylindrical waves [4]. Basic macroscopic description relying on Bloch mode excitation near the metal surface provides an approximation of the resonance frequencies [6], but fails to explain the influence of the hole size and shape, or of the plate thickness. Many models describing EET are based on mode-expansion approach [7, 8, 9, 10, 11, 12, 13, 14] or on the full resolution of Maxwell's equations [4, 15].

A Fano-like model has been adapted to EET [16, 17, 18, 19, 20], based on the similarity between EET experimental results and calculations performed by Fano on auto-ionization processes [21]. This model considers the interference between two contributions: a continuum of non-resonant states and a resonant state related to the periodic structure, both contributions being coupled together. Assuming a constant coupling as in auto-ionization, the Fano model has been successfully integrated to the EET framework, and describes the asymmetrical profiles as well as the interaction between surface waves [22, 20] but it fails to describe in details the influence of the geometry and the origin of the coupling.

In this paper, based on experimental measurements in the terahertz domain on arrays of subwavelength holes, we found that the coupling between resonant and non-resonant states is Gaussian, and therefore showed that the hypothesis of constant coupling is not valid for EET. We present an analytical extension of the Fano model of EET incorporating for the first time geometrical considerations such as the size and shape of the subwavelength apertures.

2. Extended Fano model

Fano introduced in 1961 a model describing auto-ionization processes of helium [21]. It has now been extended to many other fields such as quantum wires, mesoscopic transport phenomena, polariton in inhomogeneous absorptive dielectric, or transmission coefficient in an Aharonov-Bohm ring [23, 24]. Fano described the scattering process of an electron through both a continuum of states and an isolated state, coupled together. The model relies on basic quantum physics, and describes the two paths that the electron can choose: the non resonant

#111238 - $15.00 USD Received 11 May 2009; revised 30 Jun 2009; accepted 30 Jun 2009; published 14 Aug 2009

one through the continuum, and the resonant one via the isolated level. The calculus leads to a transmission related parameter equal to the ratio of probability of taking the first over the second path.

A parallel can be drawn between the Fano model and EET. Two choices are available for light impinging the array of subwavelength holes. First, light can go through by being diffracted by the aperture, as was first described by Bethe [25, 26]. Considering an impinging wave, diffraction by the subwavelength aperture generates a continuum of high spatial frequency wave vectors. Second, light can couple to the surface and cross the screen via the surface waves, interacting with the periodic structure as given by Bloch model. Therefore, the transmission process involves a non resonant continuum of scattered states (the incident wave diffracted by the apertures) and a resonant state (Bloch model). After propagation through the array, both components coherently interfere and it results in a new plane wave since apertures are subwavelength. Even though the high spatial frequency wave vectors vanish after full propagation through the array, their coupling with the periodic structure is responsible for the resonance of EET. Schematically (see figure 1), the system is described by an initial state $|i\rangle$ and excited state $|\psi_E\rangle$. The latter is the result of the coupling between a non resonant continuum $\{|E\rangle\}$ and a resonant state $|\varphi\rangle$. Without coupling between $\{|E\rangle\}$ and $|\varphi\rangle$, the matrix elements of the non perturbed Hamiltonian H_0 are

$$\langle\varphi|H_0|\varphi\rangle = E_\varphi \quad (1)$$

$$\langle E|H_0|E'\rangle = E\,\delta(E-E'), \quad (2)$$

where δ is the Dirac function. Considering a coupling between $\{|E\rangle\}$ and $|\varphi\rangle$, the total Hamiltonian becomes

$$H = H_0 + V, \quad (3)$$

where V is the coupling Hamiltonian. $|\psi_E\rangle$ are the eigenstates of H of eigenvalues E and the new matrix elements are

$$\langle E|V|\varphi\rangle = v(E) \quad (4)$$

$$\langle E|V|E'\rangle = \langle\varphi|V|\varphi\rangle = 0. \quad (5)$$

Now, we consider the coupling between an initial state $|i\rangle$ and either the discrete or continuum states. The transmission efficiency through the periodic arrays of subwavelength holes is then given by the probability of transition from $|i\rangle$ to the final state $|\psi_E\rangle$ with coupling, $|\langle\psi_E|T|i\rangle|^2$, normalized by the transition probability in absence of coupling, $|\langle E|T|i\rangle|^2$. According to Fano derivation [21], one obtains

$$T(E) = \frac{|\langle\psi_E|T|i\rangle|^2}{|\langle E|T|i\rangle|^2} = \frac{[q(E)+\varepsilon(E)]^2}{1+\varepsilon^2(E)}, \quad (6)$$

with

$$\varepsilon(E) = \frac{E-E_\varphi-\Gamma(E)}{\pi v^2(E)}, \quad (7)$$

and $q(E)$ the Breit-Wigner-Fano coupling coefficient defined as

$$q(E) = \frac{\langle\varphi|T|i\rangle}{\pi v^*(E)\langle\psi_E|T|i\rangle}. \quad (8)$$

The parameter Γ is related to the coupling Hamiltonian matrix element by a Hilbert transform as

$$\Gamma(E) = \pi\,\mathrm{Hilb}[|v(E)|^2] = \mathrm{PP}\int\frac{|v(E')|^2}{E-E'}\,dE', \quad (9)$$

#111238 - $15.00 USD Received 11 May 2009; revised 30 Jun 2009; accepted 30 Jun 2009; published 14 Aug 2009

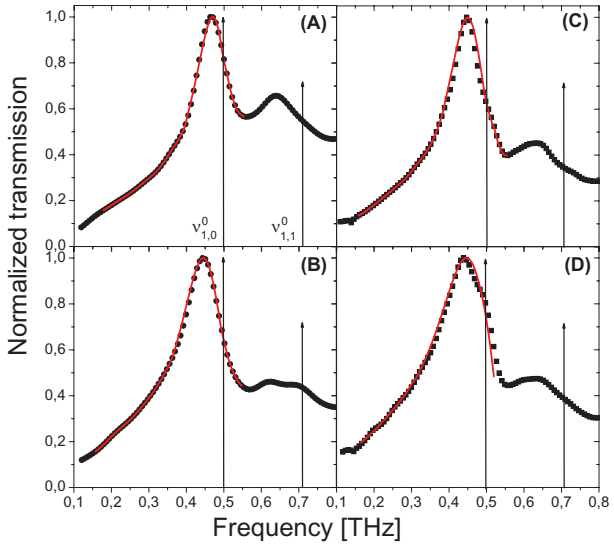

Fig. 2. Normalized transmission spectra of subwavelength hole arrays ($L = 600\,\mu$m), for round holes of diameter $270\,\mu$m (**A**) and $350\,\mu$m (**B**), and for square holes of effective hole diameter (see text for definition) of $233\,\mu$m (**C**) and $273\,\mu$m (**D**). The black dots are the experimental data and the red solid lines come from the extended Fano model using eq. 6 and 15, and the parameters A and Δ are found in figures 4 and 5. The arrows show Bloch model frequencies as $\nu^0_{i,j} = \frac{c}{L}\sqrt{i^2+j^2}$ where i and j are integers [1].

where PP stands for "principal part of".

The physical interpretation of these parameters is as follows: E_φ corresponds to the resonance energy from Bloch model as $E_\varphi = h\nu^0_{i,j}$ with $\nu^0_{i,j} = \frac{c}{L}\sqrt{i^2+j^2}$ where i and j are integers [1] ; $v^2(E)$ provides the resonance width, correlated by a Hilbert transform to the resonance shift $\Gamma(E)$. Finally, the dimensionless ratio $q(E)$ is a shape factor controlling the asymmetry of the resonance. In his original model, Fano made strong assumptions that were valid for autoionization, namely that q, v and Γ were supposed to be independent of E over the considered range. In the case of EET, these assumptions are not *a priori* justified and taking into account the possible dependence with respect to E could provide new parameters to describe EET more precisely.

3. Experimental results

The enhanced transmission through the subwavelength hole arrays was measured by Terahertz Time-Domain Spectroscopy (THz-TDS) from 0.1 to 2 THz [27]. Thanks to the very long wavelength of the radiation ($300\,\mu$m at 1 THz), the corresponding mechanical precision on the hole geometry allows a very accurate design and shape control of the apertures. Therefore, polyhedral geometries can be investigated: triangle, square, pentagon and round holes of various sizes. Broadband linearly polarized subpicosecond single cycle pulses of terahertz radiation are generated and coherently detected by illuminating photoconductive antennas with two synchronized femtosecond laser pulses. Numerical Fourier transform of the time-domain signals gives access to the transmission spectrum of the arrays. The samples are free-standing 10-μm-thick nickel arrays of subwavelength polyhedral holes, fabricated by electroforming. Influence

#111238 - $15.00 USD Received 11 May 2009; revised 30 Jun 2009; accepted 30 Jun 2009; published 14 Aug 2009

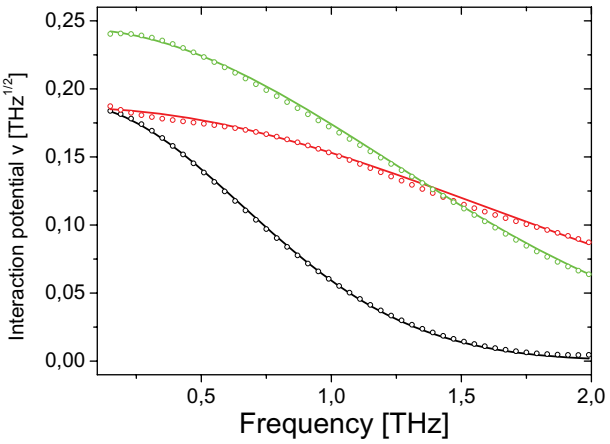

Fig. 3. Coupling Hamiltonian matrix element $v_E(E)$ calculated from experimental data (dots) and Gaussian fit (solid line), for round (hole diameter: 210 μm, black) and square (effective hole diameter 113 μm, green and 194 μm, red) apertures. The Laguerre decomposition used is truncated at fifth order ($k=5$, $n=10$, see Appendix A).

of substrate or plate thickness is then negligible, and the plates are still much thicker than skin depth in the terahertz range. All arrays have a $L=600\,\mu$m period, and are positioned on a 10 mm circular aperture, in the linearly polarized, frequency independent 4.8 mm-waist (1/e in amplitude) Gaussian THz beam. The precision over the hole size and periodicity is 1 μm. The dynamics of the EET is then recorded during 250 ps, yielding to a 4 GHz frequency precision after numerical Fourier transform, with 10^4 signal to noise ratio in a 300 ms acquisition time. A reference scan is taken with empty aperture. The transmission of the array is then calculated by taking the amplitude ratio of the complex spectra of the metal plate and reference scans.

Typical spectra can be found in Figure 2, for round and square apertures. Each spectrum exhibits typical EET features, with non-symmetrical resonance profiles [19]. In first approximation, the resonances can be found at frequencies given by Bloch theory as $\nu^0_{i,j}$. The observed resonance frequencies $\nu_{i,j}$ are shifted from $\nu^0_{i,j}$ as usually found [20, 28, 29]. In order to compare holes of various shapes, we introduced an effective hole diameter D for which $S=\pi D^2/4$ equals the real surface of an individual hole. Contrary to some previous papers, we do not observe anti-resonance at Bloch frequencies, probably due to the ultra thin metal plates used in the experiments.

The key point is the fitting procedure of Eq. 6 applied to the terahertz spectra, for various hole sizes and for round, square, triangle and pentagon apertures. Details may be found in the appendix A. Parameters q and v are left free to evolve with respect to E. The first important result is that parameter q remains constant for all shapes and sizes, within experimental uncertainty ($q=-6\pm0.5$). On the contrary, v is not constant, and exhibits a strong dependence with E. It then appears that q is no more an important parameter of our model. The peak asymmetry will be much more sensitive now to the simultaneous evolution of $v(E)$ and $\Gamma(E)$ rather than q. The coupling Hamiltonian is clearly of Gaussian shape, whose height and width depend on the shape and size of the apertures, as shown in figure 3. $v(E)$ can then be written in terms of Gaussian parameters, as

$$v(E)=\frac{2}{\sqrt{\pi}}\frac{A}{\Delta}e^{-E^2/\Delta^2}. \tag{10}$$

#111238 - $15.00 USD Received 11 May 2009; revised 30 Jun 2009; accepted 30 Jun 2009; published 14 Aug 2009

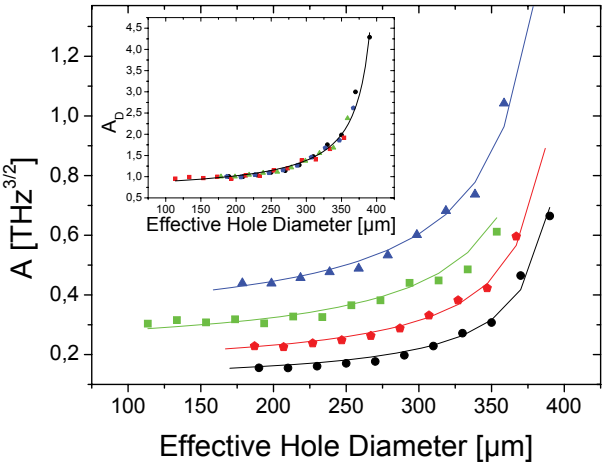

Fig. 4. Evolution of the amplitude A of the Gaussian coupling (see Eq. 10) versus effective hole diameter for round (black), pentagon (red), square (green) and triangle (blue) apertures. The inset shows the evolution of the normalized parameter A_D for all aperture shapes. Solid lines are fits from equation 12.

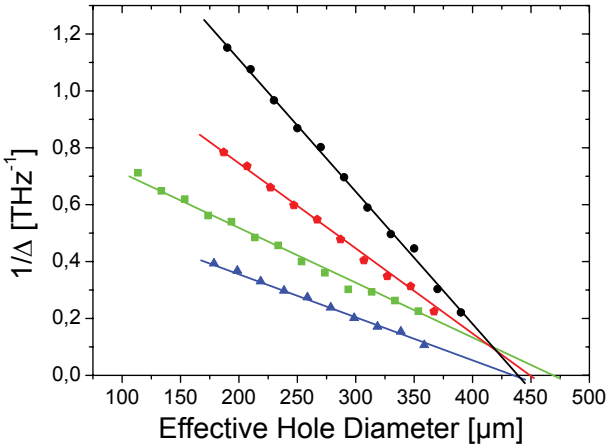

Fig. 5. Evolution of the inverse of width of the Gaussian coupling $1/\Delta$ (see Eq. 10) versus effective hole diameter for round (black), pentagon (red), square (green) and triangle (blue) apertures. Solid lines are linear fits.

Parameter A represents the integral of the Gaussian, as $A = \int_0^\infty v(E)dE$, and Δ is the width of the Gaussian. Since $v^2(E)$ has the dimension of an energy (taken in THz for purpose of simplicity here), dimensions of A and Δ are then in $\mathrm{THz}^{3/2}$ and THz, respectively. Evolution of Gaussian parameters A and Δ can be found in figures 4 and 5.

Parameter A evolves monotonously with respect to D (see figure 4). Moreover, its profile is the same for all the hole shapes. Every curves can be superimposed within uncertainty range if normalized. This parameter can then be decomposed into shape-dependent and size-dependent

#111238 - $15.00 USD Received 11 May 2009; revised 30 Jun 2009; accepted 30 Jun 2009; published 14 Aug 2009

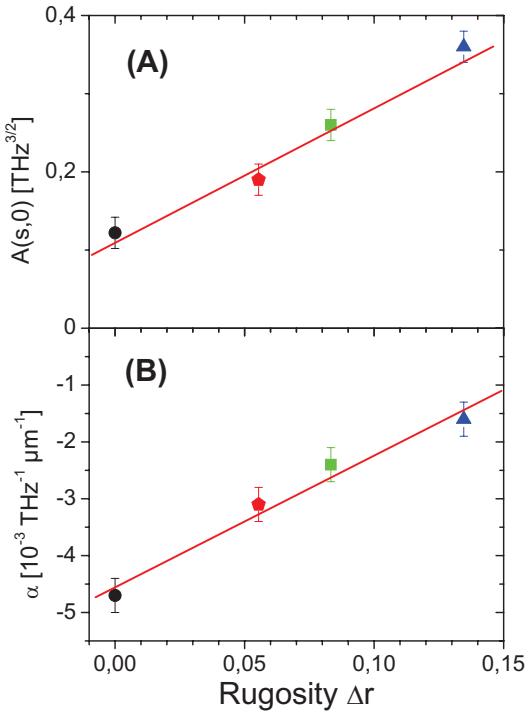

Fig. 6. Evolution of the amplitude of the coupling $A(s,0)$ and slope $\alpha(s)$ of the inverse of width of the coupling $1/\Delta$ versus aperture rugosity Δr. Solid lines are linear fits. The 4 markers correspond to the 4 different hole shapes.

functions as

$$A(s,D) = A(s,0) \times A_D(D), \tag{11}$$

where s refers to round, square, triangle or pentagon shapes. We found that all the curves are homothetic to a unique hyperbolic function. The inset of figure 4 shows $A_D(D)$ and the solid curve is a fit with the following hyperbolic function

$$A_D(D) = 0.75 - 105/(D-413), \tag{12}$$

with D in μm. Evolution of the shape-dependent parameter $A(s,0)$ is also given by figure 6A. To compare the different hole shapes, a rugosity parameter Δr has been introduced as the mean deviation of the hole profiles compared to the mean radius $\bar{r}$,

$$\Delta r^2 = \frac{n}{2\pi}\int_0^{2\pi/n} [r(\theta)-\bar{r}]^2\, d\theta \quad \text{with} \quad \bar{r} = \frac{1}{2\pi}\int_0^{2\pi} r(\theta)\, d\theta, \tag{13}$$

where $n = 3,\ 4,\ 5$ or ∞ for triangle, square, pentagon and round shapes, respectively, and $r(\theta)$ is the polar coordinate of the hole with respect to its center. $A(s,0)$ is an increasing function of rugosity.

As for parameter Δ (see figure 5), its inverse is found to be a linear function of D. Therefore, the slope only depends on the hole shape, and one can write

$$\frac{1}{\Delta(s,D)} = -\alpha(s)[D - D(s)]. \tag{14}$$

#111238 - $15.00 USD Received 11 May 2009; revised 30 Jun 2009; accepted 30 Jun 2009; published 14 Aug 2009

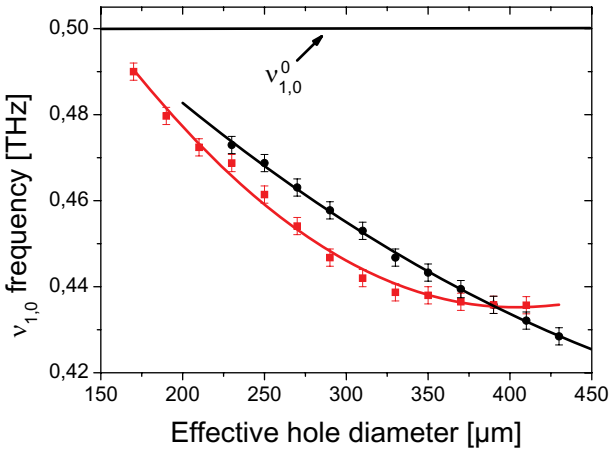

Fig. 7. Evolution of the frequency $\nu_{1,0}$ of the first resonance versus effective hole diameter for round holes (black round dots) and square holes (red square dots). Black and red solid lines are the maximum resonance from the extended Fano model for round and square holes, respectively.

Furthermore, the slope $\alpha(s)$ is an increasing linear function of the rugosity (see figure 6B). Each linear $1/\Delta$ curves crosses the X axis at a point $D(s)$ comprised between 420 and 470 μm, corresponding to a state of infinitely broad coupling Hamiltonian.

Using these parameters, expression of EET within extended Fano model can be expressed with analytical functions. The frequency shift Γ is given by the Hilbert transform of a Gaussian, as $\mathrm{Hilb}(e^{-x^2}) = -e^{-x^2}\,\mathrm{erfi}(x)$ where erfi is the imaginary error function defined as $\mathrm{erfi}(x) = -i\,\mathrm{erf}(ix)$ [30]. Then

$$\Gamma = -\frac{4A^2}{\Delta^2}\exp\left[-2\left(\frac{E}{\Delta}\right)^2\right]\mathrm{erfi}\left(\sqrt{2}\frac{E}{\Delta}\right), \tag{15}$$

which complete the analytical expression of EET using equations 6, 7, 10, 11, 12 and 14.

The use of this set of equations may be found in figures 2 and 7. The last one presents the evolution of the experimental frequency $\nu_{1,0}$ of the first resonance, compared to the one of the extended Fano model. Both show that $\nu_{1,0}$ is larger for big apertures, and converges toward $\nu^0_{1,0}$ for tiny apertures. Evolutions of $\nu_{1,0}$ for round and square hole lattice are very different, highlighting the complex relationship between EET and the geometry of the screen [29].

4. Discussion

We can infer from the Gaussian characteristic of the coupling $v(E)$ that the Hamiltonian related to the discrete state is parabolic, and that the discrete state can be simply described as an harmonic oscillator [31] (see Appendix B). As a consequence, the ground state of the discrete state can also be considered as Gaussian.

The Gaussian parameters A and Δ of the coupling Hamiltonian exhibit very interesting behavior for large hole size. Both parameters diverge for large apertures, at approximately the same effective hole diameter, even though Δ seem to diverge at diameters slightly different for each shape within experimental uncertainty. When the hole size increases, the amplitude of the coupling Hamiltonian increases, correlated with a broadening of the coupling Hamiltonian, up to a point where the validity of the model vanishes. This is in good agreement with the recent

#111238 - $15.00 USD Received 11 May 2009; revised 30 Jun 2009; accepted 30 Jun 2009; published 14 Aug 2009

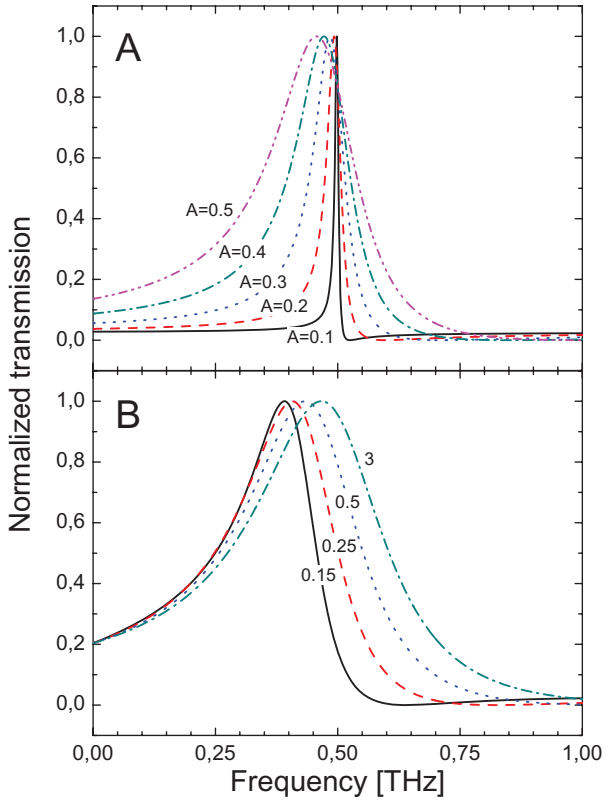

Fig. 8. Fano profiles obtained from the extended Fano model (Eq. 6). **(A)** $\Delta = 3$ and A varies from 0.1 to 0.5. **(B)** the ratio Δ/A remains constant and equal to 5, while A varies from 0.15 to 3.

observation of the disappearance of EET in subwavelength hole arrays at large hole size in round and square apertures in the terahertz regime [29]. For large holes, EET was found to be replaced by symmetric resonances scaling as integers. The transition between the two transmission modes was described as a first order phase transition at effective hole sizes of 440 and 475 μm, respectively for round and square apertures, in good correspondence with the results of figure 5 (438 and 466 μm, respectively).

This model also precisely describes the influence of the rugosity of the apertures, from sharp (triangle) to smooth (round) contours. The origin of sensitivity of the resonance to rugosity may be due to a modification of the local field distribution inside the holes, as well as a modification of the coupling between adjacent holes.

The influence of the two parameters A and Δ on the shape of the resonance is not as straightforward as in the original Fano model, since the coupling now depends on the frequency. However it is possible to obtain a general behavior of A and Δ. Figure 8 shows several calculated Fano profiles, for various values of A and Δ. It results in first order that A mainly affects the width of the resonance, with Δ constant (Figure 8A), whereas the ratio A/Δ controls the asymmetry and shift (Figure 8B).

#111238 - $15.00 USD Received 11 May 2009; revised 30 Jun 2009; accepted 30 Jun 2009; published 14 Aug 2009

5. Conclusion

Based on time-domain terahertz spectroscopy, we developed an extended analytic Fano model describing the extraordinary electromagnetic transmission through arrays of subwavelength apertures, including an energy dependent coupling Hamiltonian. The coupling is found to be Gaussian, and can be easily described as a function of the size and shape of the apertures. This model precisely predicts the influence of the hole geometry on the transmission resonance and shows the disappearing of EET characteristics for large apertures.

A. Numerical calculation of the extended Fano model parameters

The numerical parameters $v(E)$ and $q(E)$ are derived from the inversion calculation of Laplace transform [32]. The procedure is based on the decomposition of $v(E)$ over orthonormal Laguerre functions $\phi_k(E)$ defined from Laguerre polynomials $L_k(E)$ by [33]

$$\phi_k(E) = e^{-E/2} L_k(E) = e^{-E/2} \sum_{l=0}^{k} b_l E^l, \tag{16}$$

where b_l are the Laguerre polynomial coefficients. The coupling $v(E)$ is decomposed over these orthonormal functions as

$$v(E) = \sum_{k=0}^{\infty} a_k \phi_k(E). \tag{17}$$

Therefore, the Hilbert transform is given by

$$\Gamma(E) = \mathrm{PP} \int_0^{\infty} \frac{|v(u)|^2}{E-u}\, du = \mathrm{PP} \int_0^{\infty} \frac{|\sum_{k=0}^{\infty} a_k \phi_k(u)|^2}{E-u}\, du \tag{18}$$

$$= \sum_{n=0}^{\infty} c_n \int_0^{\infty} \frac{e^{-E} u^n}{E-u}\, du, \tag{19}$$

where c_n are coefficients straightforwardly obtained from the a_k and b_l coefficients. At last, the latter integral is calculated using the saddle point method [33] for any value of n. The summation is truncated at a given value of k. We carefully checked that the values of Γ rapidly converge for increasing values of k, and we assumed here that $k = 5$ (*i.e.* $n = 10$). Higher order Laguerre polynomial decomposition was checked to have negligible effect on the fitting precision, but it increases the calculation time. As a result, one obtains an expression of the transmission T using eq. 6. Transmission is then a function of q and Laguerre coefficients a_k. These parameters are calculated using the nonlinear least-square method [34] on the difference between the measured transmission and theoretical expressions (eq.6 and following), depending on parameters a_k, q and E.

The fundamental advantage of this method is that it returns an implicit form of the Hilbert transform of $v(E)$. Consequently, the value $\Gamma(E)$ is known for any desired value of E with little additional cost since most computational cost is spent in calculating the coefficients of the Laguerre expansion.

B. Harmonic oscillator model

Let H be the total Hamiltonian

$$H = H_E + H_\varphi + V, \tag{20}$$

where H_E refers to the continuum $\{|E\rangle\}$, H_φ to the resonant state $|\varphi\rangle$ and V is the coupling Hamiltonian between resonant and non-resonant states whose matrix elements are

$$v(E) = \langle E|V|\varphi\rangle. \tag{21}$$

#111238 - $15.00 USD Received 11 May 2009; revised 30 Jun 2009; accepted 30 Jun 2009; published 14 Aug 2009

Let $|\varphi\rangle$ be the resonant ground state depending on the state coordinate ρ. Since V does not depend on ρ,

$$v(E) = \langle E|V|\varphi\rangle = V_0\langle E|\varphi\rangle, \tag{22}$$

and then representing the continuum as plane waves $|E\rangle \propto e^{ik\rho}$, one obtains

$$v(E) \propto V_0 \int \varphi(\rho) e^{ik\rho}\, d\rho. \tag{23}$$

Then v and φ are related by Fourier transform. Since $v(E)$ is Gaussian, one obtains

$$\varphi = \varphi_0 e^{-\rho^2/\Delta\rho^2}. \tag{24}$$

The resonant ground state is found to be Gaussian, which is characteristic of a parabolic resonant Hamiltonian $H_\varphi = a\rho^2$.

#111238 - $15.00 USD Received 11 May 2009; revised 30 Jun 2009; accepted 30 Jun 2009; published 14 Aug 2009